Ultrafast thermoelasticity modeling of microbump formation irradiated by femtosecond laser

Zehua Han (韩泽华), Changhe Zhou (周常河), and Enwen Dai (戴恩文)

Shanghai Institute of Optics and Fine Mechanics, Chinese Academy of Sciences, Shanghai 201800

Received January 30, 2008

Finite element method and ultrafast thermoelasticity model are combined to simulate the microbump formation irradiated by a femtosecond laser. It has been shown that the effect of microbump formation is related to the characteristic of incident femtosecond laser and the thermoelasticity properties of the film. The numerical results exhibit good agreements with the experimental results in both the shape and height of the conical microbump structure, which verify the effectiveness of the ultrafast thermoelasticity model in experiments. It should be helpful for selecting appropriate materials for nanotexturing of thin films by ultrafast lasers.

OCIS codes: 140.3330, 160.3380.
doi: 10.3788/COL20080608.0619.

Ultrafast lasers are very attractive in precise material processing, especially in the fields of micromachining, microoptics, and microelectronics[1−3]. There are many particular merits of ultrafast lasers micromachining, such as negligible thermal damage to the surroundings, high cutting effiency, nearly ablation of all kinds of materials, and precise control of machining sizes. In spite of its widely applications in many areas of technology, the basic mechanisms leading to ablation or micromachining are still not understood well. Three types of two-step heating model, parabolic[4], hyperbolic[5] and dual-hyperbolic[6], have been proposed for simulating the thermal transport phenomena in metals irradiated by sub-nanosecond and shorter pulse lasers. Among these, the dual-hyperbolic two-temperature model is the most general version for describing the evolutions of both the electron and lattice temperatures during ultrafast lasers micromachining. However, none of above mentioned models refers to the non-thermal high stress damage mechanisms. Recently, Chen *et al.* developed a new ultrafast thermoelasticity model (UTEM) based on the dual-hyperbolic two temperature and hot-electron blast models[7]. In this letter, we combined the finite element method (FEM) and the UTEM to simulate the microbump formation on Cr film irradiated by a femtosecond laser and compared the results with the experimental results.

We undertake an attempt to describe the phenomenon of microbump formation appeared on the nanosize Cr films irradiated by a femtosecond laser. The fully coupled, nonlinear, transient thermoelasticity equations that govern ultrafast thermomechanical response for a metal film in three-dimensional (3D) space are given as follows[7]:

$$\rho\ddot{u}_i = \sigma_{ji,j} + 2\Lambda T_{\rm e} T_{{\rm e},i}, \qquad i,j = 1,2,3, \tag{1}$$

$$C_{\rm e}\dot{T}_{\rm e} = -q_{{\rm e}i,i} - G(T_{\rm e} - T_{\rm l}) + S, \tag{2}$$

$$\tau_{\rm e}\dot{q}_{{\rm e}i} + q_{{\rm e}i} = -K_{\rm e} T_{{\rm e},i}, \tag{3}$$

$$C_{\rm l}\dot{T}_{\rm l} = -q_{{\rm l}i,i} + G(T_{\rm e} - T_{\rm l}) - (3\lambda + 2\mu)\alpha T_{\rm l}\dot{\varepsilon}_{ii}, \tag{4}$$

$$\tau_{\rm l}\dot{q}_{{\rm l}i} + q_{{\rm l}i} = -K_{\rm l} T_{{\rm l},i}, \tag{5}$$

where ρ indicates the mass density of the materials, u_i are the displacements of the lattices, σ_{ij} are the stresses, Λ is the coefficient for the hot-electron blast force, T is the temperature, C is the heat capacity, q_i is the heat flux vector, G is the electron-lattice coupling factor, S is the volumetric laser heat source, τ is the relaxation time, K is the thermal conductivity, λ is the Laméconstant, ν is the shear modulus, α is the thermal expansion coefficient, and ε_{ij} are the strains. The subscripts i, j and k ($= 1, 2, 3$ for each) refer to the spatial coordinates in 3D space. The quantities with subscripts e and l are associated with the electron and lattice, respectively.

The volumetric laser heat source with a Gaussian temporal and spatial profile is expressed as

$$S(r,z,t) = \sqrt{\frac{\beta}{\pi}}\frac{(1-\delta)J_0}{t_{\rm p} z_{\rm s}} \times \exp[-(\frac{r}{r_{\rm s}})^2 - (\frac{z}{z_{\rm s}}) - \beta(\frac{t-2t_{\rm p}}{t_{\rm p}})^2], \tag{6}$$

where r and z are the radial and axial (thickness) coordinates respectively, J_0 is the laser fluence, δ is the surface reflectivity, $t_{\rm p}$ is the laser pulse duration, $r_{\rm s}$ is the spot radius, $z_{\rm s}$ is the penetration depth including ballistic range, and the constant $\beta = 4\ln 2$. The magnitude of the hot-electron blast force coefficient is estimated by Falkovsky *et al.*[8]

$$\Lambda = gC_{\rm e0} \cong C_{\rm e0}, \tag{7}$$

where $C_{\rm e0}$ is a constant characteristic in the electron heat capacity $C_{\rm e}(T_{\rm e})$[9],

$$C_{\rm e}(T_{\rm e}) = C_{\rm e0} T_{\rm e}. \tag{8}$$

The electron relaxation time $\tau_{\rm e}$ is a function of electron and lattice temperatures[10]

$$\tau_{\rm e} = \frac{1}{A_{\rm e}T_{\rm e}^2 + B_{\rm l}T_{\rm l}}, \tag{9}$$

where $A_{\rm e}$ and $B_{\rm l}$ are constants. The electron thermal conductivity $K_{\rm e}$ is expressed in the form[11]

$$K_{\rm e} = \chi\frac{(\phi_{\rm e}^2 + 0.16)^{5/4}(\phi_{\rm e}^2 + 0.44)\phi_{\rm e}}{(\phi_{\rm e}^2 + 0.092)^{1/2}(\phi_{\rm e}^2 + \eta\phi_{\rm l})}, \tag{10}$$

where $\phi_e \equiv T_e/T_F$ and $\phi_l \equiv T_l/T_F$ are the normalized electron and lattice temperatures with T_F denoting the Fermi temperature, χ and η are material constants. The phonon relaxation time τ_l is given by[12]

$$\tau_l = \frac{3K_l}{C_l V_s^2}, \tag{11}$$

with V_s being the speed of sound.

Considering a metal film heated by an ultrafast Gaussian laser pulse is at rest and at a uniform room temperature initially, the initial conditions are

$$u_i(r,z,0) = 0, \quad \dot{u}_i(r,z,0) = 0, \tag{12}$$

$$\sigma_{ij}(r,z,0) = 0, \tag{13}$$

$$T_e(r,z,0) = T_l(r,z,0) = 300 \text{ K}, \tag{14}$$

$$q_{ei}(r,z,0) = q_{li}(r,z,0) = 0. \tag{15}$$

During the short time period of the laser heating, heat losses to the surrounding boundary as well as to the front and back surfaces of the metal film are assumed to be negligible, implying the following boundary conditions:

$$q_{ei}(r,0,t) = q_{ei}(r,L,t) = q_{ei}(R,z,t) = 0, \tag{16}$$

$$q_{li}(r,0,t) = q_{li}(r,L,t) = q_{li}(R,z,t) = 0, \tag{17}$$

where L is the film thickness, and R is the radius of the surrounding boundary. For the mechanical response, it is assumed that the front and back surfaces of the film are stress free while the surrounding boundary is constrained. This gives

$$\sigma_{ij}(r,0,t) = \sigma_{ij}(r,L,t) = 0, \tag{18}$$

$$u_i(R,z,t) = 0. \tag{19}$$

Equations (1)—(5) was solved by the FEM, in which the finite element matrix equation for the conservation of momentum, Eq. (1), is written as[7]

$$[m]\{\ddot{u}\} + [k]\{u\} = \{f_{T_l}\} + \{f_{T_e}\}, \tag{20}$$

where $\{\ddot{u}\}$ and $\{u\}$ are the nodal acceleration and displacement vectors, $[m]$ and $[k]$ are the mass and stiffness matrices, $\{f_{T_l}\}$ and $\{f_{T_e}\}$ are the classical thermal load vector that results from the non-uniform lattice temperature and the hot-electron blast force vector, respectively. In each time step, the time rates of change of the temperatures are first determined from the energy Eqs. (2) and (4), and then the temperatures are advanced using the finite element meshes. Once the temperatures are obtained, the rates of change of the heat fluxes are computed from the constitutive Eqs. (3) and (5). Subsequently, the heat fluxes are updated using the finite element meshes. With the current temperatures and the heat fluxes, the nodal displacements $\{u\}$ are solved from the finite element Eq. (20) by using the constant acceleration Newmark time integration scheme[13]. After the stresses are evaluated, the above solution procedure repeats for the next time step.

Square Cr film with a thickness $L = 145$ nm irradiated by Gaussian laser pulses is considered in the numerical analysis. The centre of the beam cross-section coincides with the centre of the front surface of the film. The femtosecond laser pulse is assumed to have a pulse duration of 100 fs at the wavelength of 800 nm. The thermophysical and thermoelastic properties of Cr used in the modeling are as follows[14]: $\rho = 7190$ kg/m^3, $C_{e0} = 194$ J/(m^3·K^2), $G = 4.2\times10^{17}$ W/(m^3·K), $\delta = 0.631$, $z_s = 24$ nm, $\chi = 300$ W/(m·K), $\eta = 0.20$, $T_F = 8.01\times10^4$ K, $C_l = 3.24\times10^6$ J/(m^3·K), $K_l = 0$ W/(m·K), $\Lambda = 194$ J/(m^3·K^2), $E = 248$ GPa, $\nu = 0.40$, and $\alpha = 19.5\times10^{-6}$ K^{-1}.

Figures 1 and 2 present the simulant deformation of Cr film irradiated by a 100-fs, 800-nm femtosecond laser pulse at two different fluences. It can be seen that conical microbump structure is formed on the surface of Cr film. The height of the microbump is 139 nm at the fluence of 0.8 J/cm^2 and is 208 nm at the fluence of 1.4 J/cm^2. The height of the microbump increased with the fluence nonliearly is due to the electron blast force which is not linearly changed with the fluence according to the UTEM. Figure 3 shows the schematic representation of the process of microbump formation induced by a femtosecond laser. In the process of deformation, the irradiated zone on the film gains thermalelastic stress normal to the substrate surface. The deformation of the film becomes plastic when the stress is beyond the yield stress of the material, which makes the film cannot restore its initial shape and results in the formation of microbump after the femtosecond laser irradiation. When the stress gets so large that it cannot be extinguished by the plastic deformation with the increment of the fluence, the material will eject from the surface and result in ablation of the film. Figure 4 exhibits the experimental surface morphology and profile of the Cr film irraditated by a

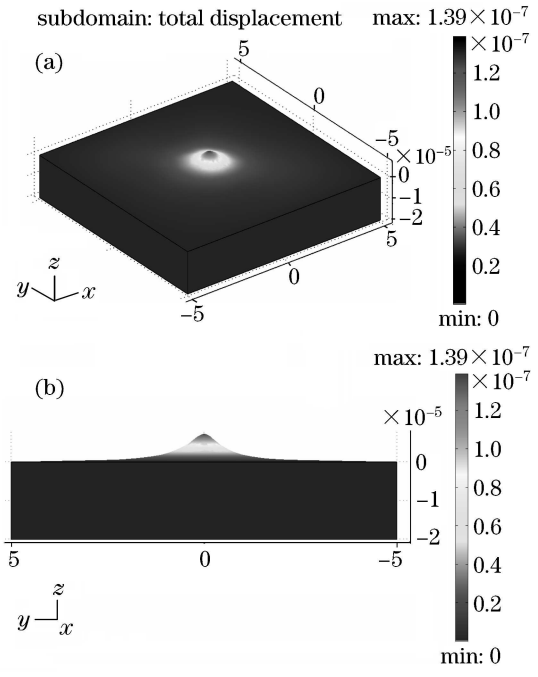

Fig. 1. Simulant deformation of Cr film irradiated by a 100-fs, 800-nm femtosecond laser pulse at the fluence of 0.8 J/cm^2. (a) 3D view and (b) cross section view.

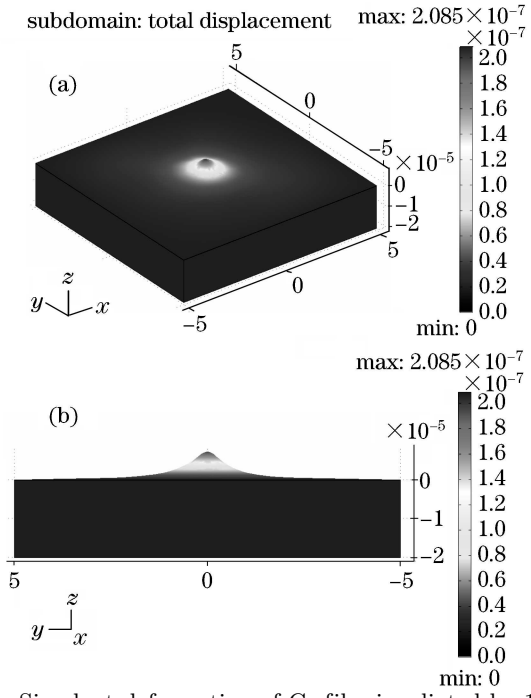

Fig. 2. Simulant deformation of Cr film irradiated by 100-fs, 800-nm femtosecond laser pulse at the fluence of 1.4 J/cm^2. (a) 3D view and (b) cross section view.

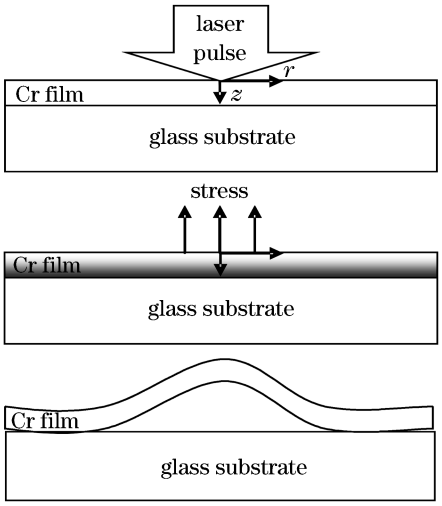

Fig. 3. Schematic representation of the process of microbump formation.

100-fs, 800-nm femtoseond laser pulse at the fluence of 1.4 J/cm^2. It can be seen that the nearly conical microbump structure is appeared on the surface of Cr film and has a height of 230 nm, which shows good agreements with the simulant result in Fig. 2 for both the shape and height of the conical microbump structure. It has verified the reasonableness and effectiveness of the UTEM in experiments. Furthermore, the materials with small elastic modulus such as Au, Ag and Cu will get a higher microbump structure under the same irradiation condition according to the numerical simulant results.

In conclusion, the FEM and UTEM were combined to simulate the microbump formation on Cr film irradiated by a femtosecond laser. The simulant results showed that the effect of microbump formation was related to the characteristic of incident femtosecond laser and the thermoelasticity properties of the film. It exhibited good agreements with the experimental results in both the shape and height of the conical microbump structure, which verified the reasonableness and effectiveness of the UTEM in experiments. It should be helpful for nanotexturing of thin films by ultrafast lasers.

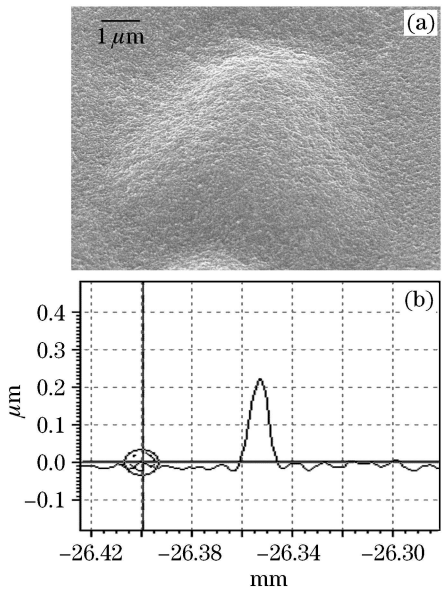

Fig. 4. (a) Experimental surface morphology and (b) profile of the Cr film irraditated by a 100-fs, 800-nm femtoseond laser pulse at the fluence of 1.4 J/cm^2.

This work was supported by the Shanghai Science and Technology Committee (No. 06SP07003 and 0652nm005) and the National "973" Program of China (No. 2006CB806000). Z. Han's e-mail address is zhhan@semi.ac.cn.

References

1. H. Zhang, S. M. Eaton, J. Li, and P. R. Herman, Opt. Lett. **31,** 3495 (2006).
2. P. Srisungsitthisunti, O. K. Ersoy, and X. Xu, J. Opt. Soc. Am. B **24,** 2090 (2007).
3. Y. Li, H. Jiang, H. Yang, and Q. Gong, Chin. Opt. Lett. **3,** S200 (2005).
4. S. I. Anisimov, B. L. Kapeliovich, and T. L. Perelman, Sov. Phys. JETP **39,** 375 (1974).
5. T. Q. Qiu and C. L. Tien, J. Heat Transfer **115,** 835 (1993).
6. J. K. Chen and J. E. Beraun, Numer. Heat Transfer Part A **40,** 1 (2001).
7. J. K. Chen, J. E. Beraun, and C. L. Tham, Int. J. Eng. Sci. **42,** 793 (2004).
8. L. A. Falkovsky and E. G. Mishchenko, J. Exp. Theor. Phys. **88,** 84 (1999).
9. C. Kittle, *Introduction to Solid State Physics* (Wiley, New York, 1967).
10. X. Y. Wang, D. M. Riffle, Y. S. Lee, and M. C. Downer, Phys. Rev. B **50,** 8016 (1994).
11. S. I. Anismov and B. Rethfeld, Proc. SPIE **3093,** 192 (1997).
12. D. Y. Tzou, *Macro- to Microscale Heat Transfer: The Lagging Behavior* (Taylor and Francis, Washington D. C., 1997).
13. K.-J. Bathe, *Finite Element Procedures* (Prentice-Hall, New Jersey, 1996).
14. B. S. Yilbas, J. Phys. D **35,** 1210 (2002).